Provenance of Baker River sediments (Chile, 48°S): Implications for the identification of flood deposits in fjord sediments

Abstract

Floods are among the most destructive natural hazards on Earth. In paleohydrology, sediments are generally considered as one of the best archives to extend flood records to pre-historical timescales. Doing so requires being able to identify flood deposits from sediment archives and decipher between flood types. The latter is particularly important in glacierized regions, where meteorological floods frequently co-occur with Glacial Lake Outburst Floods (GLOFs). In Patagonia, results from a recent study suggest that GLOFs are recorded in downstream fjord sediments as fine-grained and organic-poor layers, representing the high amount of glacier rock flour transported during lake outbursts, whereas meteorological floods are represented by coarser and more organic deposits. However, not all fine-grained organic-poor deposits could be associated with historical GLOFs. Here, we reconstruct the provenance of these Baker River flood deposits using $^{87}Sr/^{86}Sr$ and εNd, taking advantage of the clear lithological differences that exist between both sides of the watershed. Our results show that both $^{87}Sr/^{86}Sr$ and εNd are suited to reconstruct sediment provenance in the Baker River watershed but that εNd is the most effective and the least affected by grain-size variations. Our provenance results confirm that the 21st century fine-grained and organic-poor deposits represent GLOFs and that the largest winter meteorological flood on record has a distinct coarse and organic-rich signature. However, our results show that rain-on-snow events that occur in summer, and therefore primarily affect the western glacierized part of the watershed, have the same fine-grained organic-poor signature as GLOFs. Therefore, this study shows that the sedimentary signature of rain-on-snow floods in partially glacierized watersheds depends on the season during which they occur. We anticipate that our findings will contribute to a better interpretation of flood records from partially glacierized watersheds.

Keywords: Glacial Lake Outburst Floods, rain-on-snow floods, Patagonia, paleohydrology, grain size, Nd isotopes, Sr isotopes

1. Introduction

Floods are arguably one of the most catastrophic hydrological hazards on Earth. These ubiquitous events can cause enormous economic loss and casualties (e.g., Hirabayashi et al., 2013) and the ongoing intensification of the hydrological cycle is expected to result in an increase in both their frequency and magnitude at various locations globally (Kundzewicz et al., 2014; Breugem et al., 2020). In glacierized regions, meteorological floods frequently co-occur with Glacial Lake Outburst Floods (GLOFs), i.e., floods caused by the sudden emptying of ice- or moraine-dammed lakes (e.g., Carrivick & Tweed, 2016). As the number and size of glacial lakes are currently increasing worldwide (Shugar et al., 2020), it is urgent to understand how GLOFs respond to climate change to assess how their frequency and magnitude will evolve in a future warmer world.

The lower Baker River watershed (47–48°S) in Chilean Patagonia is particularly vulnerable to both meteorological floods and GLOFs (Dussaillant et al., 2010, 2012; Iribarren Anacona et al., 2014; Jacquet et al., 2017; Vandekerkhove et al., 2020b; Benito et al., 2021). This results from the hyperhumid climate that is typical of Chilean Patagonia (Garreaud et al., 2013), and from the abundance of glacial lakes formed by the recession of outlet glaciers, primarily from the Northern Patagonian Icefield (NPI) (Davies & Glasser, 2012; Wilson et al., 2018). Until recently, most of the historical GLOFs that occurred in the lower Baker River watershed were thought to have originated from the Colonia River, due to the abrupt draining of either Cachet II or Arco lakes (e.g., Harrison & Winchester, 2000; Dussaillant et al., 2010; Jacquet et al., 2017). However, recent studies indicate that at least one historical GLOF within the Baker River watershed originated from a smaller moraine-dammed lake not related to the NPI (Iribarren Anacona et al., 2014; Vandekerkhove et al., 2021).

One of the best archives of Baker River floods are the sediments deposited in the fjord immediately downstream of the Baker River (Martínez Channel). Based on a comparison of sedimentological data with historical chronicles, Vandekerkhove et al. (2021) showed that the 21st century GLOFs originating from Lake Cachet II were recorded in the fjord's sediments as fine-grained and organic-poor deposits. This is in contrast with the common idea that floods are consistently recorded in sediments as turbidites (e.g., Schillereff et al., 2014; Wilhelm et al., 2015) but it accurately reflects the release of large amounts of glacier rock flour in Baker River during GLOFs. Older Martínez Channel sediments also contain fine-grained organic-poor deposits and turbidites relatively rich in organic matter, which were tentatively attributed to GLOFs and meteorological floods, respectively, by Vandekerkhove et al. (2021). However, based on sedimentological and chronological criteria only, several of these flood layers could not be attributed to historical flood events, rendering the conclusions about the exact signature of GLOFs and meteorological floods relatively uncertain.

Properly interpreting flood deposits in terms of specific flood type is crucial to generate independent records of meteorological floods and GLOFs, and therefore use these records to acquire a mechanistic understanding of the factors affecting flood occurrence. Such an objective calls for a detailed investigation of sediment provenance. Being able to track sediment provenance is also of prime importance to understand the lake or icefield at the origin of each GLOF. This is particularly relevant in Patagonia, where glaciers may respond differently to climate according to their longitudinal position (precipitation-driven vs ablation-driven; e.g., Bertrand et al., 2012a).

With this in mind, this study aims to reconstruct the provenance of Baker River flood deposits preserved in the sediments of Martínez Channel using Sr and Nd isotopes. These two geochemical tracers reflect the type and age of the source rocks (Faure and Mensing 2004) and they are particularly suited for fine-grained siliciclastic sediments (Jonell et al., 2018). They are also known to accurately reflect the differences in the bedrock lithologies that occur in western Patagonia (Liu et al., 2020). To achieve this goal, we first compare the isotopic signature of suspended sediments from the largest tributaries to the lithology of the bedrock in their respective watersheds, and we use these results to define the sediment end-members. We then investigate the influence of grain size on Sr and Nd isotopes using measurements obtained on eight grain-size fractions separated from a bulk river sediment sample from the Baker River mouth. Finally, we use Sr and Nd isotopes to reconstruct the provenance of historical (1975–2017) flood deposits of known and unknown origin identified in a sediment core from the head of Martínez Channel. The provenance results are then compared with historical data to refine the sedimentological interpretation of the deposits. We anticipate that our results will constitute a strong basis for future paleohydrological research in glacierized regions, including the generation of independent meteorological flood and GLOF proxy records.

2. Setting

2.1 Study area

Baker River is the largest river in Chile in terms of mean annual discharge (Dussaillant et al., 2012). It originates at Lake Bertrand and it discharges in Martínez Channel near the town of Tortel (Figure 1), where it forms a large subaquatic delta incised by submarine channels (Vandekerkhove et al., 2020a). The Baker River watershed is relatively large (29,202 km^2) and it comprises numerous icefields and glaciers, including several outlet glaciers of the Northern Patagonian Icefield (NPI) in the west, the San Lorenzo icefield in the southeast, and smaller mountain glaciers, including those of the Cordon de los Ñadis (Figure 1). Due to the input of large amounts of glacial meltwater in summer, Baker River shows sizeable variations in discharge with seasons, ranging from 600 m^3/s in winter to 1200 m^3/s in summer (Dussaillant et al., 2012). Baker River is fed by several large proglacial rivers originating from NPI outlet glaciers on the western side of the watershed, such as Colonia River, and by smaller rivers from the east, some of which are proglacial in nature (e.g., the del Salto and los Ñadis rivers).

In addition to Baker River, three other large rivers discharge at the head of the Baker-Martínez fjord system: Huemules River, which originates from Steffen Glacier at the southern end of the NPI; Bravo River, which drains a relatively small watershed to the east of the fjord complex, and Pascua River, which is the outflow of Lake O’Higgins and is fed by meltwater from the Southern Patagonian Icefield (SPI) (Figure 1).

The Baker River watershed presents a wide range of environments that mostly reflect the strong west-to-east gradients in precipitation and, to a lesser extent, elevation and therefore surface temperature. The western part of the watershed is characterized by a cold and hyperhumid climate, with annual precipitation reaching 3000–4000 mm/yr, whereas its eastern part across the border with Argentina is warmer and semi-arid, with precipitation dropping below 500 mm/yr (Garreaud et al., 2013; Fick & Hijmans, 2017).

The sediment budget of Baker River is dominated by particles originating from its lower watershed, i.e., downstream of Bertrand and Cochrane lakes (Figure 1). This sub-division in upper and lower watersheds (Figure 1) mostly reflects the ability of lakes General Carrera and Cochrane to trap most of the sediment produced in the upper watershed. The main sources of sediment to Baker River are therefore located in the lower watershed, which is composed of two main lithological units (Figure 1) (SEGEMAR, 1998; SERNAGEOMIN, 2003; Gómez et al., 2019): the Patagonian Batholith (PB), which is located to the west and is composed of Cretaceous to Miocene granitoids, and the Eastern Andean Metamorphic Complex (EAMC) to the east. Although the PB and EAMC are each composed of lithologies of distinct ages, the exact distribution of the sub-units is not reported in the literature (e.g., Pankhurst et al., 1999; Augustsson & Bahlburg, 2003). Volcanic rock formations crop out in the eastern part of the watershed and thick fluvioglacial deposits marking the maximum Quaternary extent of the Patagonian Ice Sheet occur in the easternmost part of the watershed in Argentina (Boex et al., 2013; Kaplan et al., 2005). It is worth noting that the location of Baker River roughly corresponds to the limit between the PB and EAMC lithologies (Figure 1). Therefore, all proglacial rivers originating from NPI outlet glaciers (e.g., Huemules and Colonia rivers) predominantly drain the PB, whereas those to the east, including Chacabuco, del Salto, and los Ñadis, mostly drain the EAMC (Figure 1; Table 1). To the south, the Bravo River watershed and the lower Pascua River watershed, i.e., downstream of the large Lake O'Higgins, are almost entirely composed of EAMC (Figure 1; Table 1).

2.2 Flood history

Historical Baker River floods consist of GLOFs and meteorological floods. According to historical and instrumental information, most recent GLOFs originated from the Colonia River and were due to the drainage of either Lake Arco (until the 1960s) (e.g., Harrison & Winchester, 2000; Dussaillant et al., 2010), or Lake Cachet II (from 2008 onwards) (e.g., Jacquet et al., 2017; Vandekerkhove et al., 2021). Between 2008–2017, a sequence of 21 GLOFs caused by the sudden emptying of Lake Cachet II occurred (Dussaillant et al., 2010, 2012; Jacquet et al., 2017). During these events, the Baker River tripled in discharge (Dussaillant et al., 2010), and its suspended sediment concentration increased 8-fold, transporting considerable amounts of sediments (1.0–1.5 x 10^5 tons per GLOF event) to the head of Martínez Channel (Quiroga et al., 2012). Local testimonies and satellite images also indicate the existence of a GLOF from proglacial lake Las Lengas, in the los Ñadis valley (Figure 1), in March 1988 (Iribarren Anacona et al., 2014; Vandekerkhove et al., 2021). This event resulted in a significant increase in the discharge of los Ñadis River (Iribarren Anacona et al., 2014), but its signature in the Baker River hydrographs is unclear, possibly due to their low temporal resolution (one measurement daily; Vandekerkhove et al., 2021).

Due to relatively high year-round precipitation and the presence of large icefields and mountain glaciers, this region is also prone to meteorological floods driven by extreme precipitation, high seasonal meltwater discharge, and rain-on-snow events (Dussaillant et al., 2012; Vandekerkhove et al., 2021). Two particularly large rain-on-snow events occurred in December 1976 and December 1989 (Dussaillant et al., 2012). Another large meteorological flood, possibly also corresponding to a rain-on-snow event, was identified in August 1992 (Vandekerkhove et al., 2020b). During those events, the discharge of Baker River (2000–3000 m^3/s) reaches values similar to peak discharge during GLOFs (2000–4000 m^3/s; Dussaillant et al., 2012; Vandekerkhove et al., 2021).

3. Material and Methods

3.1. Material

3.1.1 River suspended sediments

Water samples were collected at the mouths of (a) the two largest NPI proglacial rivers (i.e., Huemules and Colonia rivers), (b) four rivers mainly draining the EAMC (i.e., del Salto, los Ñadis, Bravo and Pascua rivers), and (c) Baker River, in Jan–Feb 2019 (Figure 1). To obtain a sufficient amount of suspended sediment (>100 mg) for analysis, around 100 L of water was collected at the center of each river ~20 cm below the surface, either using a telescopic rod with a 2L beaker from a riverbank (Colonia River), or using a bucket from a bridge (del Salto and los Ñadis rivers) or from a boat (Huemules, Baker, Bravo, and Pascua rivers).

All water samples were filtered through a 0.22 μm PES membrane using a pre-rinsed pressurized filtration system. The suspended sediments were kept frozen until processing in the laboratory. They were then separated from the filters by repeated washing with Milli-Q water and ultrasonic bathing. Subsequently, the suspended sediments were freeze-dried and stored in glass vials. The volume of filtered water and the weight of dry suspended sediment were used to calculate suspended sediment concentrations (SSC).

3.1.2 Bulk river sediments

Bulk river sediment sample RS11-05 was collected from a recently abandoned meander near the mouth of Baker River in November 2011 (Figure 1) and separated into eight grain-size fractions. The fractions coarser than 32 μm (i.e., 32–45, 45–63, 63–90, and 90–125 μm) were separated by dry sieving, whereas the finer fractions (0–4, 4–8, 8–16 and 16–32 μm) were obtained after sedimentation in Atterberg columns following Stokes' law. Sediments coarser than 125 μm were not investigated since they are not representative of the fraction that reaches the fjord (Bertrand et al., 2012b; Vandekerkhove et al., 2020a).

3.1.3 Fjord sediments

A 106.8 cm-long sediment core (FC17-08) collected at the head of Martínez Channel approximately 5 km off the Baker River mouth (Figure 1) was subsampled for this study. This sediment core was obtained on the delta slope at a depth of 207 m using a gravity corer operated from the R/V Sur Austral in February 2017. It is the most representative of a set of ten sediments cores collected at the fjord head (Vandekerkhove et al., 2021). An age-depth model was constructed based on ^{210}Pb measurements made at a 10 cm interval on the turbidite-free sediments (i.e., after removing the turbidite at 66–70 cm). A Constant Flux-Constant Sedimentation

(CFCS) model was used to generate the core chronology (Vandekerkhove et al., 2021). According to the age-depth model, FC17-08 covers the period 1982–2017, with sedimentation rates ranging between 2.88 and 3.03 cm/yr (Figure 2). Prior to this study, the sediment core was described, scanned on a Geotek multisensor core logger and on an XRF core scanner, and analyzed for grain size and total organic carbon (TOC) content (Vandekerkhove et al., 2021).

Sediment core FC17-08 is mostly composed of homogeneous silt-sized particles, with intercalations of fine mud layers between 0–27.5 cm and at 82–83 cm, and of a fine-grained turbidite at 66–70 cm (Figure 2). The fine mud layers are typically finer (mean grain size: 5.98 ± 0.82 μm) and less organic (TOC: 0.31 ± 0.06 %) than the background sediment (mean grain size: 7.32 ± 0.65 μm, TOC: 0.36% ± 0.04 %). The turbidite, however, is relatively rich in organic matter (0.57 ± 0.10 %). The mud deposits that occur between 0–27.5 cm have a modeled age of 2008–2017 and were interpreted as the signature of the 21st century Cachet II GLOFs (Vandekerkhove et al., 2021). The turbidite between 66–70 cm (modeled age 1990–2000) was tentatively interpreted as the signature of the 1992 rain-on-snow event, mostly based on its age, but it could also correspond to the 1988 Las Lengas GLOF (Vandekerkhove et al., 2021). The fine mud deposit at 82–83 cm (modeled age 1984–1997) was however associated with more certainty with the 1988 Las Lengas GLOF by Vandekerkhove et al. (2021).

To investigate the provenance of these deposits, a total of seven subsamples were taken from sediment core FC17-08 (Figure 2): two representing background sediments at 51.0–51.5 and 75.0–75.5 cm; three corresponding to the fine-grained 2008–2017 Cachet II GLOF deposits at 17.0–17.5, 24.0–24.5 and 26.0–26.5 cm; and two in unknown event deposits: one near the base of the turbidite at 69.0–69.5 cm; and one in the fine mud layer at 82.0–82.5 cm.

3.2 Methods

3.2.1 Sr and Nd isotopes

The seven river suspended sediment samples, the eight grain-size fractions of Baker River sediment sample RS11-05, and the seven subsamples from sediment core FC17-08 were analyzed for Sr and Nd isotope ratios at the University of Missouri Research Reactor (MURR), Columbia MO, USA. About 100 mg of sample was digested in 1 mL 14 N HNO_3 + 4 mL 24 N HF, and 6 mL 5–6 N HCl, successively, using several cycles of heating and evaporation. Subsequently, 2 mL 14 N HNO_3 was added to the residues for dissolution and evaporation, followed by 1.5 mL 2 M HNO_3 for final dissolution. The Sr and Nd fractions were then extracted following a protocol slightly modified from Míková & Denková (2007), using chromatographic columns that were homemade out of Pasteur pipets with a 4 mm internal diameter.

The Sr and Nd isotope analyses were conducted on a Nu Plasma II MC-ICP-MS. Analytical conditions are reported in Supporting Information (Text S1). The Sr isotopic results obtained on reference material SRM987 (0.710256 ± 24 [2 sd]) were in agreement with recommended values (Thirlwall, 1991; De Muynck et al., 2009).

The average value obtained for the Nd isotopic standard JNdi-1 was 0.512087 ± 11 (2 sd).

The Nd isotopic compositions were expressed as εNd, which is defined as:

$$\varepsilon Nd = [(^{143}Nd/^{144}Nd)_{sample}/(^{143}Nd/^{144}Nd)_{CHUR} - 1] \times 10^4$$

where $(^{143}Nd/^{144}Nd)_{CHUR}$ is the value of the Chondritic Uniform Reservoir (0.512638; Jacobsen & Wasserburg, 1980).

The isotopic composition of the sediment samples was compared to the composition of the main bedrock lithologies occurring in their watersheds. These values were collated from the literature, i.e., Pankhurst et al. (1999) for the PB and Weaver et al. (1990) for the EAMC.

3.2.2 Grain-size analysis

Grain size was measured on the river suspended sediment samples and on the eight grain-size fractions of RS11-05 using a Malvern Mastersizer 3000 at Ghent University. The grain size of the suspended sediment sample from Bravo River was not measured due to limited sample amount. Organic matter, carbonate, and biogenic silica were removed by sequentially boiling the sample suspended in 10 mL DI water with 2 mL 30% H_2O_2, 1 mL 10% HCl and 1 mL 2 N NaOH, respectively. Each sample was then boiled with 1 mL 2% sodium hexametaphosphate for complete disaggregation before analysis. Sample amount was adjusted to reach a laser beam obscuration between 5 and 15%. The geometric mean of the grain size distributions was calculated with GRADISTAT v.8 (Blott & Pye, 2001). The same procedure was used by Vandekerkhove et al. (2021) to measure the grain size of the FC17-08 subsamples.

3.2.3 Statistical analysis

To investigate the possible influence of sediment grain-size on the Sr and Nd isotopic composition of the river and fjord sediment samples, the relations between grain size, Sr and Nd isotopes, and bulk mineralogy (measured by XRD and semi-quantified using RockJock v.11; Liu et al., 2019) of the eight grain-size fractions of river sediment sample RS11-05 were examined by PCA using XLSTAT 2019. To overcome the close-sum effect and the non-negative nature of compositional data (Aitchison, 1986, 1990), grain-size mean was expressed in phi units, and mineralogical data were transformed to centered log-ratios.

4. Results

4.1 River suspended sediments

The seven river suspended sediment samples display $^{87}Sr/^{86}Sr$ and εNd values that are distinctive from each other (Figure 3a). The suspended sediment samples obtained from the proglacial rivers mainly draining the PB lithology (i.e., Huemules and Colonia rivers) show relatively low $^{87}Sr/^{86}Sr$ and high εNd values (Figure 3a). By comparison, the river suspended sediments from watersheds dominated by the EAMC (i.e., del Salto, los Ñadis, Bravo, and Pascua rivers) are more radiogenic in Sr, but their εNd values are generally lower (Figure 3a). The Baker River suspended sediment sample displays $^{87}Sr/^{86}Sr$ and εNd values in-between those of the Colonia and Huemules samples. The $^{87}Sr/^{86}Sr$ values are negatively correlated to the areal proportion of PB in the river's watersheds ($r = -0.67$, $p<0.1$), whereas the εNd values show a stronger and positive correlation with PB proportions ($r = 0.80$, $p<0.05$; Figure 3b).

In terms of grain size, all river suspended sediment samples are composed of clay and silt, with a mean grain size varying between 3.27 μm for the Colonia River and 7.58 μm for del Salto (Figure 4a). Overall, samples from NPI proglacial rivers (Colonia and Huemules) are finer (mean: 3.27 and 3.67 μm) than those from the eastern part of the lower Baker River watershed (del Salto and los Ñadis; mean: 7.58 and 5.54 μm). The Baker River suspended sediment sample is intermediate (mean: 4.53 μm), and its grain-size distribution is similar to that of Pascua River (mean: 4.41 μm).

4.2 Baker River sediment grain-size fractions

The eight grain-size fractions of Baker River sediment sample RS11-05 show an overall decrease in $^{87}Sr/^{86}Sr$ as grain size increases (Figures 4b, 5a). The relation between εNd and grain size is not as consistent. A decrease in εNd values is observed from clay to fine silt, followed by an increase from fine silt to sand. εNd values are the highest in the coarsest grain-size fractions.

To further investigate the grain-size control on $^{87}Sr/^{86}Sr$ and εNd of sediment, the mean grain size of each of these fractions and their isotopic and mineralogical composition was analyzed by PCA (Figure 5b). In the PCA biplot, PC1 explains

46.77% of the total variance. It displays strong positive loadings for $^{87}Sr/^{86}Sr$ and total clay minerals, and a distinct negative loading for quartz and mean grain size, providing evidence that Sr isotopes consistently covary with grain size. PC2, which accounts for 30.17% of the total variance, shows strong positive loadings for εNd, K-feldspar, and pyroxene, and distinct negative loadings for amphibole and plagioclase. εNd is positively related to K-feldspar and pyroxene, but it is orthogonal with respect to mean grain size.

4.3 Sediment core subsamples

For the FC17-08 subsamples, the background sediments show relatively low $^{87}Sr/^{86}Sr$ and high εNd values (Figure 6a). The subsamples representing the 2008–2017 Cachet II GLOF deposits at 17.0–17.5, 24.0–24.5, and 26.0–26.5 cm display similar $^{87}Sr/^{86}Sr$ and slightly lower εNd values (Figure 6a). The sample from the 66–70 cm turbidite shows very high $^{87}Sr/^{86}Sr$ and low εNd values, making it isotopically distinct from all the other subsamples. The subsample from the fine-grained and low-TOC deposit at 82–83 cm shows an isotopic composition similar to that of the 2008–2017 Cachet II GLOF deposits.

All seven sediment core subsamples are composed of clay- and silt-sized particles (Figure 4a). The background sediment samples are slightly coarser (mean: 7.73 ± 0.73 μm) than the other subsamples (Figure 4a), and those corresponding to the 2008–2017 Cachet II GLOFs are the finest (mean: 5.05 ± 0.46 μm). The two unknown event deposits are also fine-grained, with the subsample from the base of the 66–70 cm turbidite being slightly coarser (mean: 7.40 µm) than the sample from the 82–83 cm event deposit (mean: 6.04 µm). Surprisingly, the subsample representing the turbidite is finer than the background sediments (Figure 4a).

5. Discussion

5.1 River suspended sediments

The $^{87}Sr/^{86}Sr$ and εNd composition of the river suspended sediments is significantly correlated to the areal proportions of the PB and EAMC lithologies in their respective watersheds (Figure 3b). The samples from the Huemules and Colonia rivers, which drain a watershed predominantly composed of PB granitoids (Figure 1), have $^{87}Sr/^{86}Sr$ and εNd signatures that superimpose on those of the PB (Figure 3a). Likewise, the isotopic composition of the suspended sediment samples from del Salto, los Ñadis, Bravo, and Pascua rivers reflects the EAMC that dominates in their watersheds (Figures 1, 3a; Table 1). The Baker River suspended sediment sample is the only one that seem in slight disagreement with the lithology of its watershed. Its isotopic composition appears similar to that of the PB (Figure 3a), although 58% of its watershed is composed of EAMC (Table 1; Figure 3b). This can be explained by (1) the season of sample collection (summer), which likely resulted in a proportionally higher contribution of meltwater, and therefore glacial sediments from NPI proglacial rivers, (2) the high amount of sediment produced by glacier erosion, compared to the non-glacierized part of the watershed, and (3) the significantly (~3x) higher precipitation in the western part of the watershed. This is supported by the high SSC values (57–96 mg/L) that were measured in NPI proglacial rivers (Colonia and Huemules) compared to those draining the weakly-glacierized sub-watersheds to the east of Baker River (4–32 mg/L; del Salto and los Ñadis; Supplementary Information Figure S1).

Differences in $^{87}Sr/^{86}Sr$ and εNd compositions also exist between the river suspended sediments that drain watersheds of apparently similar lithology. This is particularly marked in εNd for the rivers draining the PB (Huemules and Colonia), but it is also clearly expressed in the $^{87}Sr/^{86}Sr$ and εNd signatures of the four rivers that drain EAMC-dominated watersheds (del Salto, Pascua, Bravo, los Ñadis) (Figure 3). For the Huemules and Colonia rivers, this isotopic difference most likely results from the relatively large age, and therefore isotopic, variations that occur within the PB. The PB is indeed composed of granitoids formed throughout the Cretaceous (Pankhurst et al., 1999), which covers a timespan of almost 100 Ma. However, the clear isotopic difference between the Colonia and Huemules rivers could also be explained by a non-negligible EAMC contribution for the Colonia sample since this lithology accounts for 9% of its watershed but is absent from the Huemules River watershed (Table 1). This EAMC influence is however considered minimal since most of the sediment transported by Colonia River is of glacial origin, especially in summer, and that glaciers only occur in the western part of the Colonia River watershed, which is entirely composed of PB granitoids (Figure 1).

Likewise, there are two possible explanations for the isotopic differences between the four rivers that drain EAMC-dominated watersheds. One is that the isotopic composition of the EAMC, which was formed during the Paleozoic (Weaver et al., 1990; Augustsson & Bahlburg, 2003; Moreno & Gibbons, 2007), varies across watersheds. This is however unlikely given that the samples that plot the most apart in the εNd vs. $^{87}Sr/^{86}Sr$ diagram (del Salto and los Ñadis; Figure 3a) are from rivers that drain watersheds that are adjacent (Figure 1) and that their bedrock was formed between 320–330 Ma (e.g., Augustsson & Bahlburg, 2008). The second and more likely explanation is that the suspended sediments from the del Salto and Pascua rivers receive a significant PB contribution. Indeed, the glacierized regions at the head of del Salto River and in the upper Pascua River watershed are underlain by the PB (Figure 1), and glaciers are known to significantly enhance erosion (Quinteros et al., 2004; Carretier et al., 2013), resulting in a disproportionate contribution from ice-covered lithologies (Liu et al., 2020). Therefore, the PB contribution is likely much higher than suggested by its low areal proportion, especially in summer when the suspended sediment samples were collected. The isotopic difference that exists between the del Salto and Pascua river suspended sediment samples likely results from the trapping of large amounts of glacial sediment of PB origin in Lake O'Higgins, since PB in the Pascua watershed only occurs in the upper sub-watershed (Figure 1).

5.2 End-member definition

The clear distribution of the PB and EAMC lithologies in the Baker River watershed and the overall agreement between the isotopic composition of the river suspended sediments and that of the bedrock lithologies allow us to use $^{87}Sr/^{86}Sr$

and εNd to define the sources of the fjord sediments preserved at the head of Martínez Channel. The isotopic composition of the Huemules and Colonia River suspended sediments were used to represent sediment originating from the western side of Baker River. The del Salto, los Ñadis, Bravo, and Pascua River suspended sediments were selected to define the isotopic composition of sediments originating from the eastern part of the watershed (Figure 3a). The Baker River suspended sediment sample was not used for end-member characterization since it is composed of a mixture of sediment originating from both the PB and EAMC. Although this selection makes use of samples from rivers that do not flow into Baker River to define the end-members of sediments transported by Baker River, this choice is justified by the clear distribution of the bedrock lithologies (Figure 1), and the higher number of datapoints allows us to better reflect the possible spatial and temporal variations in the nature of the sediment sources. To account for the variable $^{87}Sr/^{86}Sr$ and εNd signatures of the individual river suspended sediment samples, the range (min–max) of isotopic values was used to define the source end-members (Figure 3a).

5.3 Grain-size influence on Sr and Nd isotopes

In addition to provenance, the Sr and Nd isotopic composition of sediments is also known to be influenced by grain size (Revel-Rolland et al., 2005; Bouchez et al., 2011; Meyer et al., 2011; Jonell et al., 2018). Being able to estimate the extent of the grain-size influence on the Sr and Nd isotopic composition of sediment samples is particularly important in paleohydrology since flood deposits are typically identified by their distinctive grain-size signature (e.g., Schillereff et al., 2014; Xu et al., 2014;

Wilhelm et al., 2015). This also applies to the deposits interpreted as representing GLOFs in the sediments of the Martínez Channel since these event deposits are systematically finer than the background sediments (Vandekerkhove et al., 2021) (Figure 2).

The $^{87}Sr/^{86}Sr$ values of the Baker River sediment subsamples almost systematically decrease with grain size (Figure 5a). This trend is also visible in the PCA biplot (Figure 5b), where $^{87}Sr/^{86}Sr$ negatively covaries with mean grain size. A similar relation has been observed in other environments (e.g., Feng et al., 2009; Bouchez et al., 2011; Gili et al., 2017; Jonell et al., 2018), where it was explained by one or a combination of the following reasons: (1) mineralogical sorting during sediment transport (e.g., Garçon et al., 2013, 2014), (2) chemical weathering (e.g., Feng et al., 2009), and/or (3) differences in the provenance of the different grain-size fractions (e.g., Singh et al., 2008). For the Baker River sediments, the most plausible hypothesis is mineralogical sorting. This is supported by the covariance between $^{87}Sr/^{86}Sr$ and total clays (Figure 5b). As Rb is preferentially associated with clay minerals, the decay product of ^{87}Rb, i.e., ^{87}Sr, tends to be enriched in clays (e.g., Wedepohl, 1978), leading to high $^{87}Sr/^{86}Sr$ values in fine-grained sediments. It is also possible that the relation between $^{87}Sr/^{86}Sr$ and grain size reflects changes in the provenance of the different grain-size fractions. As shown in Figure 4b, finer sediments seem to be enriched in particles from the metamorphic complex. This hypothesis, however, is not supported by the grain size of the river suspended sediment samples, as the finest particles transported by Baker River tend to be produced by glacial erosion of the PB. Chemical weathering is the least likely reason since northwestern Patagonia has experienced limited chemical weathering, due to the cold climate and the relatively recent deglaciation (e.g., Bertrand et al., 2012b).

By comparison, the highest εNd values occur in the finest (0–4 μm) and coarsest (63–90 and 90–125 μm) fractions, with lower values in-between (Figure 5a). This trend is also reflected in the PCA biplot, which shows a weak positive covariance between εNd and mean grain size (Figure 5b). In sediments, most of the Nd isotopic budget is thought to originate from monazite/allanite (e.g., Garçon et al., 2014; Jonell et al., 2018). These two dense accessory minerals commonly occur in granites but are rare in low-grade metamorphic rocks (Anthony et al., 2000). In Baker River sediments, these two minerals therefore most likely originate from the PB. The rest of the Nd isotopic budget is generally associated with clay minerals, mostly mica (Nelson, 1988; Pankhurst et al., 1999), which is also abundant in the granitoids of the PB (Hervé et al., 1993). Therefore, the high εNd value in the finest grain-size fraction of RS11-05 likely reflects the predominant PB origin of this fraction, mostly produced by glacial erosion (cf. the grain-size distribution of the Colonia River suspended sediment sample in Figure 4a). As the grains become coarser, the dense monazite/allanite originating from the PB tend to enrich, resulting in higher εNd values in the coarsest grain-size fractions. In-between these two extremes, the sediment is likely dominated by minerals of EAMC origin, explaining the lower εNd values of the intermediate grain-size fractions. This relation is also visible in the PCA biplot, in which εNd positively covaries with K-feldspar and pyroxene, i.e., two minerals that are more abundant in the PB than in the EAMC (Güettner Oportus, 2017; Liu et al., 2020). It is also in agreement with the isotopic signatures of the lithological end-members, which show that the finest and coarsest grain-size fractions of RS11-05 are isotopically similar to the PB-dominated “West of Baker River” end-member (Figure 4b). Interestingly, the higher PB contribution in the finest grain-size fraction is not observed in $^{87}Sr/^{86}Sr$, implying that the influence of mineralogical sorting on $^{87}Sr/^{86}Sr$ overwhelms that of provenance of the individual grain-size fractions. This suggests that εNd is a better provenance indicator than $^{87}Sr/^{86}Sr$, in agreement with previous results obtained in different sedimentological settings (e.g., Meyer et al., 2011; Gili et al., 2017; Awasthi et al., 2018; Jonell et al., 2018). Those studies indeed indicate that $^{87}Sr/^{86}Sr$ is relatively sensitive to grain size whereas εNd is not and is therefore better suited to investigate sediment provenance.

An important observation is that the influence of grain size on the $^{87}Sr/^{86}Sr$ and εNd compositions of the Baker River bulk sediments is relatively limited compared to the isotopic differences between the two end-members (Figure 4b). According to the standard deviation of (a) the eight RS11-05 grain-size fractions, and (b) the end-members, the isotopic differences between the grain-size fractions of sample RS11-05 only account for 15% of the isotopic differences between the end-members. The real influence of grain size on the isotopic composition of the fjord sediment samples is probably lower than that since the mean grain size of the FC17-08 subsamples varies between 4.55 and 8.25 μm, which only covers the finest RS11-05 subsamples. The influence of grain-size on the isotopic composition of these samples mostly corresponds to the two finest RS11-05 subsamples (Figure 4b), which reduces the influence of grain size to 8 and 14% of the provenance signal for Sr and Nd isotopes, respectively. With this in mind, we consider that the isotopic composition of the fjord sediment samples mostly represents provenance.

5.4 Reconstructing the provenance of flood deposits

The two subsamples representing the background sediment of core FC17-08 have Sr and Nd isotopic signatures that correspond to the “West of Baker River” end-member (Figure 6). This suggests that the western part of the lower Baker River watershed constitutes the main source of sediments to the fjord, in agreement with the observation that glacierized sub-watersheds contribute relatively more to sediment budgets than their non-glacierized counterparts, due to efficient bedrock erosion by glaciers (Liu et al., 2020). For the Baker watershed, this is supported by the sediment budgets of Vandekerkhove et al. (2020b), which suggests that the rivers draining the western part of the watershed contribute roughly 15 times more to the Baker River sediment load than the eastern rivers.

The $^{87}Sr/^{86}Sr$ and εNd signatures of the three samples corresponding to the 2008–2017 GLOF deposits at 0–27.5 cm confirm that these deposits represent the abrupt drainage events that have affected Lake Cachet II, as they almost perfectly correspond to the isotopic signature of the Colonia River (Figure 6b). More importantly, these results confirm that Sr and Nd isotopes can be used to reconstruct the provenance of GLOF deposits, despite the minor influence of grain-size on the isotope results.

The sample representing the 66–70 cm turbidite that was deposited between 1990–2000 displays an isotopic signature that is clearly distinct from all the other samples (Figure 6b). Both isotopes plot in the “East of Baker River” end-member area, which suggests that this turbidite is predominately composed of sediment originating from the eastern side of Baker River. This result is in agreement with the hypothesis of Vandekerkhove et al. (2021) that this turbidite represents a rain-on-snow event that occurred in August 1992. In this case, the rain-on-snow event would have primarily affected the eastern part of the watershed since it happened in winter, when precipitation most likely fell as snow in the western part of the watershed, but as rain in the east (Figure 7a).

The isotopic signature of the fine-grained and organic-poor deposit at 82–83 cm undoubtedly shows that it originated from the western side of the Baker River watershed (Figure 6b). This contradicts the hypothesis of Vandekerkhove et al. (2021) that it represents the 1988 Las Lengas GLOF, which would have a clear EAMC signature (Figure 1). A more likely candidate is the rain-on-snow event that happened in December 1989 (Dussaillant et al., 2012). Since this rain-on-snow event happened in early summer, snow cover, and therefore erosion, predominantly occurred in the western part of the watershed (Figure 7b). As a result, this intense rain-on-snow event reworked glacier rock flour of PB origin, resulting in the deposition of fine-grained sediments with a PB geochemical signature in Martínez Channel. This interpretation is additionally supported by the association of a similar fine-grained low-TOC layer occurring deeper in two other sediment cores from the same fjord with a flood caused by an intense rain-on-snow event in December 1976 (Vandekerkhove et al., 2021).

The association of the 82–83 cm fine-grained deposit and 66-70 cm turbidite with the December 1989 and August 1992 rain-on-snow events, respectively, validates the ^{210}Pb chronology of sediment core FC17-08 made by Vandekerkhove et al. (2021) since both events are within the error bars of their modeled age (Figure 2). The real age of the events is consistently older (1–2 years) than their modeled age. This slight overestimation is confirmed by the modeled age (1980) of the December 1976 rain-on-snow event that was observed in the deepest sediments of the deepest cores (Vandekerkhove et al., 2021), resulting in a 3-year offset. This offset does not represent the delay between flood occurrence and formation of flood deposits since signal propagation in the Baker River system is typically in the order of days (Amann et al., submitted). This implies a slight (<10%) overestimation of the sedimentation rates by the CFCS model.

5.5 Implications for the sedimentary signature of GLOFs vs. meteorological floods

The striking similarities between the sedimentary and isotopic signatures of the early summer 1989 and 1976 rain-on-snow flood deposits with those of the 2008–2017 Cachet II GLOF deposits suggest that deposits due to GLOFs and rain-on-snow events occurring in summer may be difficult to differentiate based on their sedimentological characteristics. Although our results confirm that all Cachet II

GLOFs are recorded as fine-grained and organic-poor deposits and that none of them was able to trigger a turbidite at site FC17-08, they also suggest that not all fine-grained and organic-poor deposits can be interpreted as GLOFs. They can also represent rain-on-snow events occurring in (early) summer, i.e., when the only snow left in the watershed is over its mostly-glacierized western side (Figure 7b). Differentiating between these two types of floods remains challenging based on the existing sedimentological and isotopic criteria.

The association of the 66–70 cm organic-rich turbidite with the winter 1992 rain-on-snow event additionally shows that seasonality plays an important role in controlling how rain-on-snow events are recorded in fjord sediments. This issue probably affects all sedimentary basins receiving sediments from partially-glacierized watersheds, or at least watersheds with highly variable snow cover. Locations in the watershed where rain falls on snow produces more sediment than locations where rain falls directly on the ground.

Finally, our results also imply that the 1988 Las Lengas GLOF was not recorded at site FC17-08. This observation is supported by the lack of a discharge peak in the Baker River hydrographs, which was explained by Vandekerkhove et al. (2021) by the low (daily) resolution of the hydrographs, despite the 1301 m^3/sec discharge peak that was estimated for los Ñadis River (Iribarren Anacona et al., 2014). Both the water discharge and sediment yield of the 1988 Las Lengas GLOF were likely too low to significantly affect Baker River and therefore be recorded in the fjord's sediments.

6. Conclusions

This study confirms the ability of Sr and Nd isotopes to reconstruct sediment provenance in the Baker River watershed. Both isotopes can successfully differentiate sediments originating from the western and eastern sides of the watershed, suggesting that either isotope is powerful enough for provenance reconstruction in the Baker region. This excellent discrimination potential reflects the clear distribution of rocks of different age (Mesozoic granitoids and Paleozoic metamorphic complex) within the Baker River watershed. In addition, our results suggest that εNd is less affected by grain size than $^{87}Sr/^{86}Sr$. Despite a minor influence of grain size on the isotopic results (<15% of the provenance signal), $^{87}Sr/^{86}Sr$ and εNd can reliably be applied to flood deposits, whether they are mud layers or turbidites.

The provenance results indicate that the background sediments deposited at the head of Martínez Channel mostly originate from the western, glacierized, part of the watershed, reflecting the high erosion capacity of glaciers. In terms of event deposits, our results confirm the Cachet II origin of the fine-grained and organic-poor deposits preserved in the upper 27.5 cm of the sediment core. They also provide evidence that a similar deposit previously associated with the 1988 Las Lengas GLOF instead represents a rain-on-snow event that occurred in early summer 1989. In addition, our provenance analysis demonstrates that the turbidite at 66–70 cm originated from the eastern part of the watershed, allowing us to associate it with a rain-on-snow event that occurred in winter 1992.

These results have important implications for the sedimentary signature of GLOFs vs. meteorological floods. They confirm that GLOFs are systematically recorded as fine-grained organic-poor layers, as shown by Vandekerkhove et al. (2021), but they suggest that rain-on-snow flood events occurring in (early) summer may have the same signature, which reflects the glacial origin of the sediment transported by both flood types. Rain-on-snow floods occurring in winter, on the other hand, are recorded as regular meteorological floods (organic turbidites) since they only affect warmer (non-glacierized) sub-watersheds. In other words, the sedimentological signature of rain-on-snow events depends on snow cover distribution, and therefore on the season during which the flood occurs. Our results also suggest that GLOFs from smaller glacial lakes, such as Las Lengas, may not be recorded in downstream fjord sediments. We anticipate that these results will constitute a strong basis for the interpretation of flood deposits from sediment archives located in partially glacierized watersheds.

7. References

Aitchison J. 1986. The Statistical Analysis of Compositional Data. Chapman Hall, Ltd.: London, 416 p.

Aitchison J. 1990. Relative Variation Diagrams for Describing Patterns of Compositional Variability. Mathematical Geology 22: 487–511. DOI: 10.1007/BF00890330

Amann B, Bertrand S, Alvarez Garretón C, Reid B. submitted. Seasonal variations in fjord sediment grain size: A pre-requisite for hydrological and climate reconstructions in partially glacierized watersheds (Baker River, Patagonia). Journal of Geophysical Research: Earth Surface

Anthony JW, Bideaux RA, Bladh KW, Nichols MC. 2000. Handbook of Mineralogy, Volume 4. Anthony JW, Bideaux RA, Bladh KW, and Nichols MC (eds). Mineralogical Society of America: Chantilly, Virginia, USA, 680 p.

Augustsson C, Bahlburg H. 2003. Active or passive continental margin? Geochemical and Nd isotope constraints of metasediments in the backstop of a pre-Andean accretionary wedge in southernmost Chile (46°30'-48°30'S). In Tracing Tectonic Deformation Using the Sedimentary Record, McCann T and Saintot A (eds). Geological Society, London, Special Publications; 253–268.

Augustsson C, Bahlburg H. 2008. Provenance of late Palaeozoic metasediments of the Patagonian proto-Pacific margin (southernmost Chile and Argentina). International Journal of Earth Sciences 97: 71–88. DOI: 10.1007/s00531-006-0158-7

Awasthi N, Ray E, Paul D. 2018. Sr and Nd isotope compositions of alluvial sediments from the Ganga Basin and their use as potential proxies for source identification and apportionment. Chemical Geology 476: 327–339. DOI: 10.1016/j.chemgeo.2017.11.029

Benito G, Thorndycraft VR, Medialdea A, Machado MJ, Sancho C, Dussaillant A. 2021. Declining discharge of glacial lake outburst floods through the Holocene in central Patagonia. Quaternary Science Reviews 265: 106810. DOI: 10.1016/j.quascirev.2021.106810

Bertrand S, Hughen K, Lamy F, Stuut J-BW, Torrejón F, Lange CB. 2012a. Precipitation as the main driver of Neoglacial fluctuations of Gualas glacier, Northern Patagonian Icefield. Climate of the Past 8: 519–534. DOI: 10.5194/cp-8-519-2012

Bertrand S, Hughen K, Sepúlveda J, Pantoja S. 2012b. Geochemistry of surface sediments from the fjords of Northern Chilean Patagonia (44-47°S): Spatial variability and implications for paleoclimate reconstructions. Geochimica et Cosmochimica Acta 76: 125–146. DOI: 10.1016/j.gca.2011.10.028

Blott SJ, Pye K. 2001. Gradistat: A grain size distribution and statistics package for the analysis of unconsolidated sediments. Earth Surface Processes and Landforms 26: 1237–1248. DOI: 10.1002/esp.261

Boex J, Fogwill CJ, Harrison SP, Glasser NF, Hein AS, Schnabel C, Xu S. 2013. Rapid thinning of the Late Pleistocene Patagonian Ice Sheet followed migration of the Southern Westerlies. Scientific Reports 3: 1–6. DOI: 10.1038/srep02118

Bouchez J, Gaillardet J, France-Lanord C, Maurice L, Dutra-Maia P. 2011. Grain size control of river suspended sediment geochemistry: Clues from Amazon River depth profiles. Geochemistry, Geophysics, Geosystems 12: 1–24. DOI: 10.1029/2010GC003380

Breugem AJ, Wesseling JG, Oostindie K, Ritsema CJ. 2020. Meteorological aspects of heavy precipitation in relation to floods – An overview. Earth-Science Reviews 204: 103171. DOI: 10.1016/j.earscirev.2020.103171

Carretier S, Regard V, Vassallo R, Aguilar G, Martinod, J, Riquelme R, Pepin E, Charrier R, Hérail G, Farías M, Guyot J-L, Vargas G, Lagane C. 2013. Slope and climate variability control of erosion in the Andes of central Chile. Geology 41: 195–198. DOI: 10.1130/G33735.1

Carrivick JL, Tweed FS. 2016. A global assessment of the societal impacts of glacier outburst floods. Global and Planetary Change 144: 1–16. DOI: 10.1016/j.gloplacha.2016.07.001

Davies BJ, Glasser NF. 2012. Accelerating shrinkage of Patagonian glaciers from the Little Ice Age (~AD 1870) to 2011. Journal of Glaciology 58: 1063–1084. DOI: 10.3189/2012JoG12J026

De Muynck D, Huelga-Suarez G, Van Heghe L, Degryse P, Vanhaecke F. 2009. Systematic evaluation of a strontium-specific extraction chromatographic resin for obtaining a purified Sr fraction with quantitative recovery from complex and Ca-rich matrices. Journal of Analytical Atomic Spectrometry 24: 1498–1510. DOI:

10.1039/B908645E

Dussaillant A, Benito G, Buytaert W, Carling P, Meier C, Espinoza F. 2010. Repeated glacial-lake outburst floods in Patagonia: An increasing hazard? Natural Hazards 54: 469–481. DOI: 10.1007/s11069-009-9479-8

Dussaillant A, Buytaert W, Meier C, Espinoza F. 2012. Hydrological regime of remote catchments with extreme gradients under accelerated change: the Baker basin in Patagonia. Hydrological Sciences Journal 57: 1530–1542. DOI: 10.1080/02626667.2012.726993

Faure G, Mensing TM. 2004. Isotopes: principles and applications. 3rd edition, Wiley, 897 p.

Feng J, Zhu L, Zhen X, Hu Z. 2009. Grain size effect on Sr and Nd isotopic compositions in eolian dust: Implications for tracing dust provenance and Nd model age. Geochemical Journal 43: 123–131. DOI: 10.2343/geochemj.1.0007

Fick SE, Hijmans RJ. 2017. WorldClim 2: new 1-km spatial resolution climate surfaces for global land areas. International Journal of Climatology 37: 4302–4315. DOI: 10.1002/joc.5086

Garçon M, Chauvel C, France-Lanord C, Huyghe P, Lavé J. 2013. Continental sedimentary processes decouple Nd and Hf isotopes. Geochimica et Cosmochimica Acta 121: 177–195. DOI: 10.1016/j.gca.2013.07.027

Garçon M, Chauvel C, France-Lanord C, Limonta M, Garzanti E. 2014. Which minerals control the Nd-Hf-Sr-Pb isotopic compositions of river sediments? Chemical

Geology 364: 42–55. DOI: 10.1016/j.chemgeo.2013.11.018

Garreaud R, Lopez P, Minvielle M, Rojas M. 2013. Large-Scale control on the Patagonian climate. Journal of Climate 26: 215–230. DOI: 10.1175/JCLI-D-12-00001.1

Gili S, Gaiero DM, Goldstein SL, Chemale F, Jweda J, Kaplan MR, Becchio RA, Koester E. 2017. Glacial/interglacial changes of Southern Hemisphere wind circulation from the geochemistry of South American dust. Earth and Planetary Science Letters 469: 98–109. DOI: 10.1016/j.epsl.2017.04.007

Gómez J, Schobbenhaus C, Montes NE, Compilers. 2019. Geological Map of South America 2019. Scale 1:5 000 000

Güettner Oportus GA. 2017. Mineralogía y Proveniencia Sedimentaria del Complejo Metamórfico Andino Oriental, Mediante Conteo Modal y Modelamiento de Difractogramas, En Fiordo Jorge Montt y Peninsula la Carmela, XI Región de Aysén, Chile. MSc thesis Universidad Andrés Bello, 186 p.

Harrison S, Winchester V. 2000. Nineteenth- and Twentieth-Century Glacier Fluctuations and Climatic Implications in the Arco and Colonia Valleys, Hielo Patagónico Norte, Chile. Arctic, Antarctic, and Alpine Research 32: 55–63. DOI: 10.1080/15230430.2000.12003339

Hervé F, Pankhurst R, Suárez M, Cruz R. 1993. Basic magmatism in a mid-tertiary transtensional basin, Isla Magdalena, Aysen, Chile. Second ISAG symposium, Oxford (UK), 367–369 pp.

Hirabayashi Y, Mahendran R, Koirala S, Konoshima L, Yamazaki D, Watanabe S, Kim H, Kanae S. 2013. Global flood risk under climate change. Nature Climate Change 3: 816–821. DOI: 10.1038/nclimate1911

Iribarren Anacona P, Norton KP, Mackintosh A. 2014. Moraine-dammed lake failures in Patagonia and assessment of outburst susceptibility in the Baker Basin. Natural Hazards and Earth System Sciences 14: 3243–3259. DOI: 10.5194/nhess-14-3243-2014

Jacobsen SB, Wasserburg GJ. 1980. Sm-Nd isotopic evolution of chondrites. Earth and Planetary Science Letters 50: 139–155. DOI: https://doi.org/10.1016/0012-821X(80)90125-9

Jacquet J, McCoy SW, McGrath D, Nimick DA, Fahey M, O'kuinghttons J, Friesen BA, Leidich J. 2017. Hydrologic and geomorphic changes resulting from episodic glacial lake outburst floods: Rio Colonia, Patagonia, Chile. Geophysical Research Letters 44: 854–864. DOI: 10.1002/2016GL071374

Jonell TN, Li Y, Blusztajn J, Giosan L, Clift PD. 2018. Signal or noise? Isolating grain size effects on Nd and Sr isotope variability in Indus delta sediment provenance. Chemical Geology 485: 56–73. DOI: 10.1016/j.chemgeo.2018.03.036

Kaplan MR, Douglass DC, Singer BS, Ackert RP, Caffee MW. 2005. Cosmogenic nuclide chronology of pre-last glacial maximum moraines at Lago Buenos Aires, 46°S, Argentina. Quaternary Research 63: 301–315. DOI: 10.1016/j.yqres.2004.12.003

Kundzewicz ZW et al. 2014. Flood risk and climate change: global and regional perspectives. Hydrological Sciences Journal 59: 1–28. DOI: 10.1080/02626667.2013.857411

Liu D, Bertrand S, Villaseñor T, Van Dijck T, Fagel N, Mattielli N. 2020. Provenance of northwestern Patagonian river sediments (44–48°S): A critical evaluation of mineralogical, geochemical and isotopic tracers. Sedimentary Geology 408: 105744. DOI: 10.1016/j.sedgeo.2020.105744

Liu D, Bertrand S, Weltje GJ. 2019. An Empirical Method to Predict Sediment Grain Size from Inorganic Geochemical Measurements. Geochemistry, Geophysics, Geosystems 20: 3690–3704. DOI: 10.1029/2018GC008154

Meyer I, Davies GR, Stuut JBW. 2011. Grain size control on Sr-Nd isotope provenance studies and impact on paleoclimate reconstructions: An example from deep-sea sediments offshore NW Africa. Geochemistry, Geophysics, Geosystems 12: Q03005. DOI: 10.1029/2010GC003355

Míková J, Denková P. 2007. Modified chromatographic separation scheme for Sr and Nd isotope analysis in geological silicate samples. Journal of Geosciences 52: 221–226. DOI: 10.3190/jgeosci.015

Moreno T, Gibbons W. 2007. The Geology of Chile. The Geological Society: London, 440 p.

Nelson E, Bruce B, Elthon D, Kammer D, Weaver S. 1988. Regional lithologic variations in the Patagonian batholith. Journal of South American Earth Sciences 1:

239–247. DOI: 10.1016/0895-9811(88)90002-8

Palmer J. 2017. Chile's glacial lakes pose newly recognized flood threat. Science 355: 1004–1005. DOI: 10.1126/science.355.6329.1004

Pankhurst RJ, Weaver SD, Hervé F, Larrondo P. 1999. Mesozoic–Cenozoic evolution of the North Patagonian Batholith in Aysén, southern Chile. Journal of the Geological Society, London 156: 673–694. DOI: 10.1144/gsjgs.156.4.0673

Quinteros J, Jacovkis PM, Ramos VA. 2004. Modelado numérico del levantamiento orogénico y su potencial relación con clima y erosión. Mecánica Computacional XXIII: 2923–2931.

Quiroga E, Ortiz P, Gerdes D, Reid B, Villagran S, Quiñones R. 2012. Organic enrichment and structure of macrobenthic communities in the glacial Baker Fjord, Northern Patagonia, Chile. Journal of the Marine Biological Association of the United Kingdom 92: 73–83. DOI: 10.1017/S0025315411000385

Revel-Rolland M, Arnaud F, Chapron E, Desmet M, Givelet N, Alibert C, McCulloch M. 2005. Sr and Nd isotopes as tracers of clastic sources in Lake Le Bourget sediment (NW Alps, France) during the Little Ice Age: Palaeohydrology implications. Chemical Geology 224: 183–200. DOI: 10.1016/j.chemgeo.2005.04.014

Schillereff DN, Chiverrell RC, Macdonald N, Hooke JM. 2014. Flood stratigraphies in lake sediments: A review. Earth-Science Reviews 135: 17–37. DOI: 10.1016/j.earscirev.2014.03.011

SEGEMAR. 1998. Mapa Geológico de la República Argentina, escala 1:2.500.000.

SERNAGEOMIN. 2003. Mapa Geológico de Chile, escala 1:1.000.000.

Singh SK, Rai SK, and Krishnaswami S. 2008. Sr and Nd isotopes in river sediments from the Ganga Basin: Sediment provenance and spatial variability in physical erosion. J. Geophys. Res., 113, F03006. DOI:10.1029/2007JF000909

Shugar D.H., Burr A., Haritashya U.K., Kargel J.S., Watson C.S., Kennedy M.C., Bevington A.R., Betts R.A., Harrison S. and Strattman K. 2020. Rapid worldwide growth of glacial lakes since 1990. Nature Climate Change 10: 939–945. DOI: 10.1038/s41558-020-0855-4

Thirlwall MF. 1991. Long-term reproducibility of multicollector Sr and Nd isotope ratio analysis. Chemical Geology 94: 85–104. DOI: 10.1016/S0009-2541(10)80021-X

Vandekerkhove E, Bertrand S, Crescenzi Lanna E, Reid B, Pantoja S. 2020a. Modern sedimentary processes at the heads of Martínez Channel and Steffen Fjord, Chilean Patagonia. Marine Geology 419: 106076. DOI: 10.1016/j.margeo.2019.106076

Vandekerkhove E, Bertrand S, Mauquoy D, McWethy D, Torrejón F, Stammen S, Saunders KM. 2020b. Neoglacial increase in high-magnitude Glacial Lake Outburst Flood frequency, upper Baker River, Chilean Patagonia (47°S). Quaternary Science Reviews 248: 106572. DOI: 10.1016/j.quascirev.2020.106572

Vandekerkhove E, Bertrand S, Torrejón F, Kylander M, Reid, B., Saunders K. (2021). Signature of modern Glacial Lake Outburst Floods in fjord sediments (Baker River, southern Chile). Sedimentology 68 (6): 2798–2819. DOI: 10.1111/sed.12874

Weaver SG, Bruce R, Nelson EP, Brueckner HK, LeHuray AP. 1990a. The Patagonian batholith at 48°S latitude, Chile; Geochemical and isotopic variations. In Plutonism from Antarctica to Alaska, Kay SM and Rapela CW (eds). Special Paper of the Geological Society of America; 33–50. DOI: 10.1130/SPE241-p.33

Wedepohl KH. 1978. Strontium. In: Wedepohl, K H (Ed), Handbook of Geochemistry, Vol. II/4 - Elements Kr(36) to Ba(56). Springer-Verlag, Chapter 38.

Wilhelm B, Sabatier P, Arnaud F. 2015. Is a regional flood signal reproducible from lake sediments? Sedimentology 62 (4): 1103–1117. DOI: 10.1111/sed.12180

Wilson R, Glasser NF, Reynolds JM, Harrison S, Anacona PI, Schaefer M, Shannon S. 2018. Glacial lakes of the Central and Patagonian Andes. Global and Planetary Change 162: 275–291. DOI: 10.1016/j.gloplacha.2018.01.004

Xu M, Bogen J, Wang Z, Bønsnes TE, Gytri S. 2014. Pro-glacial lake sedimentation from jokulhlaups (GLOF), Blamannsisen, northern Norway. Earth Surface Processes and Landforms 40: 654–665. DOI: 10.1002/esp.3664

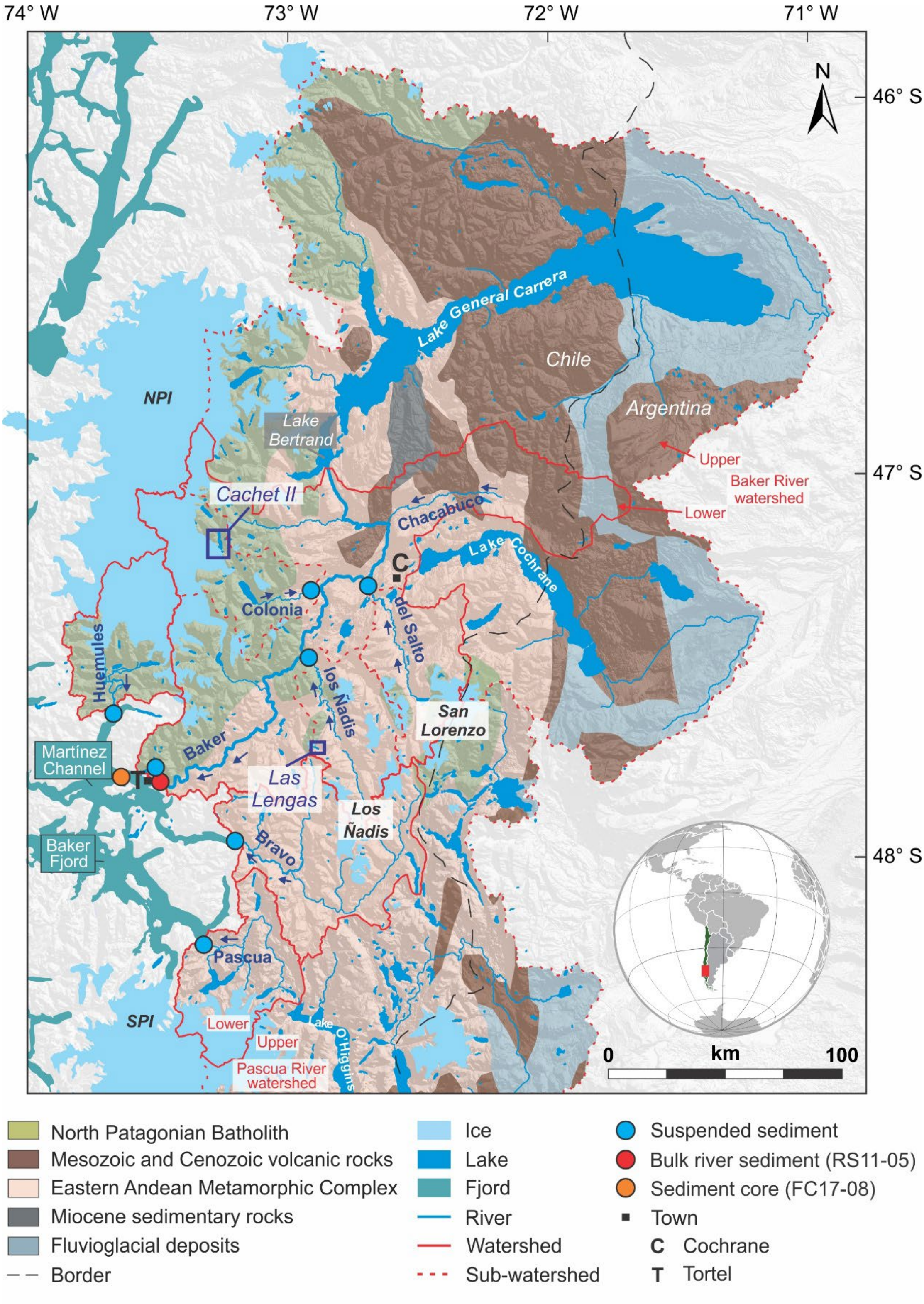

74° W
73° W
72° W
71° W
46° S
47° S
48° S
N
Lake General Carrera
Chile
Argentina
NPI
Lake Bertrand
Upper
Baker River watershed
Lower
Cachet II
Chacabuco
Lake Cochrane
C
Colonia
del Salto
los Ñadis
Huemules
San Lorenzo
Baker
Martínez Channel
T
Las Lengas
Los Ñadis
Baker Fjord
Bravo
Pascua
SPI
Lower
Upper
Pascua River watershed
Lake O'Higgins
0
km
100
North Patagonian Batholith
Mesozoic and Cenozoic volcanic rocks
Eastern Andean Metamorphic Complex
Miocene sedimentary rocks
Fluvioglacial deposits
Border
Ice
Lake
Fjord
River
Watershed
Sub-watershed
Suspended sediment
Bulk river sediment (RS11-05)
Sediment core (FC17-08)
Town
C Cochrane
T Tortel

Figure 1. Geological map of the study region in Patagonia (based on SEGEMAR, 1998, SERNAGEOMIN, 2003, and Gómez et al., 2019), showing the location of the Baker River, its tributaries, and the fjord in which it discharges (Martínez Channel). The Northern Patagonian Icefield (NPI), Southern Patagonian Icefield (SPI), San Lorenzo icefield, and Cordón de los Ñadis icefield are also shown. The two proglacial lakes that are at the origin of the Baker River historical GLOFs are indicated using dark blue rectangles. The location of the river bulk (Baker; RS11-05) and suspended (Colonia, del Salto, los Ñadis, Huemules, Baker, Bravo and Pascua River) sediment sampling sites, as well as of sediment core FC17-08, are also indicated.

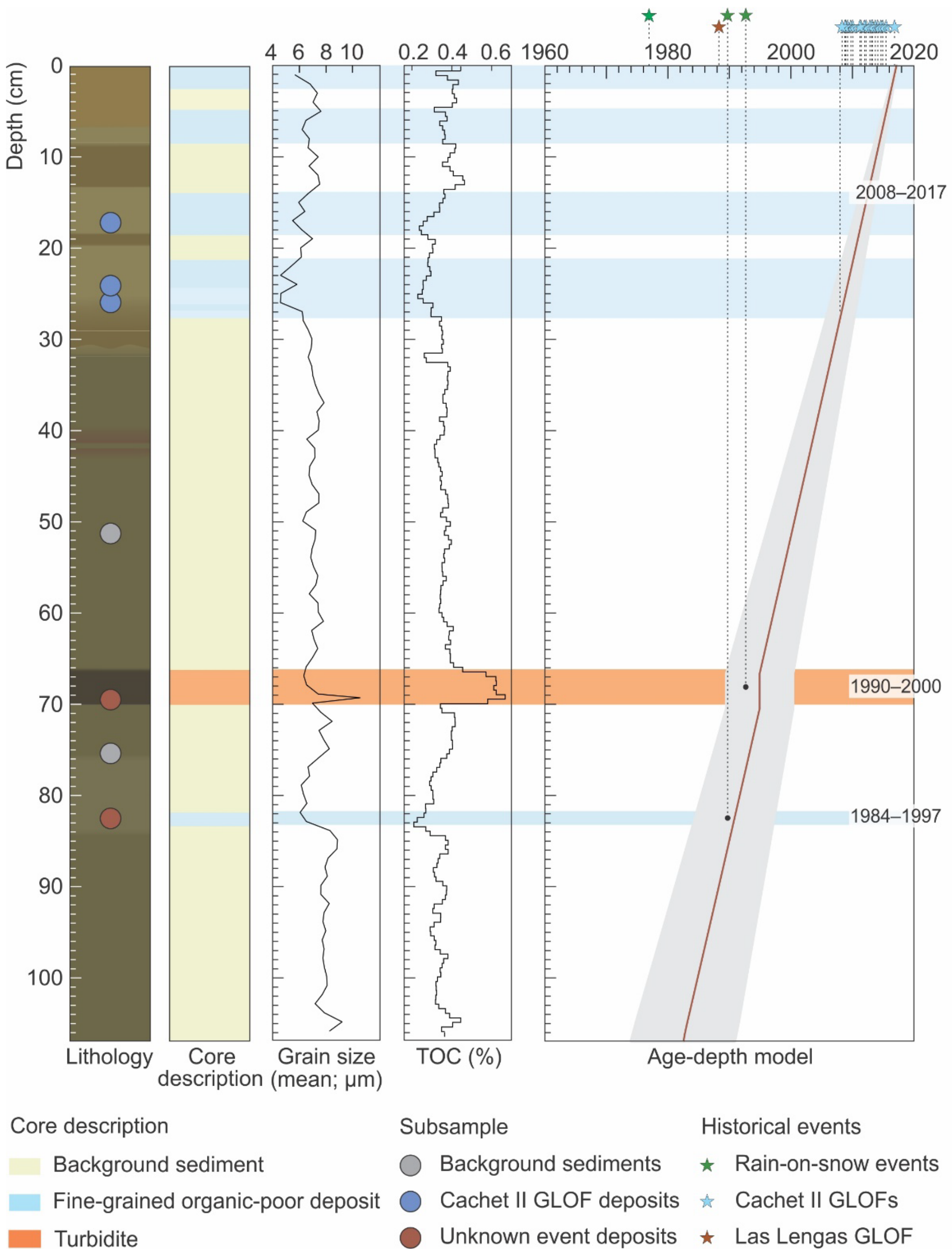

Figure 2. Lithology of sediment core FC17-08 (from Vandekerkhove et al., 2021) and location of the subsamples used in this study. The downcore variations in mean grain size and total organic carbon (TOC) confirm the identification of fine-grained organic-poor event deposits (uppermost 27.5 cm of the core and 82–83 cm) and of a relatively organic fine-grained turbidite (66–70 cm). The age-depth model (also from Vandekerkhove et al., 2021) shows that

the sediment core covers the period 2017 to 1974–1991. The modeled ages of the event deposits are shown to the right.

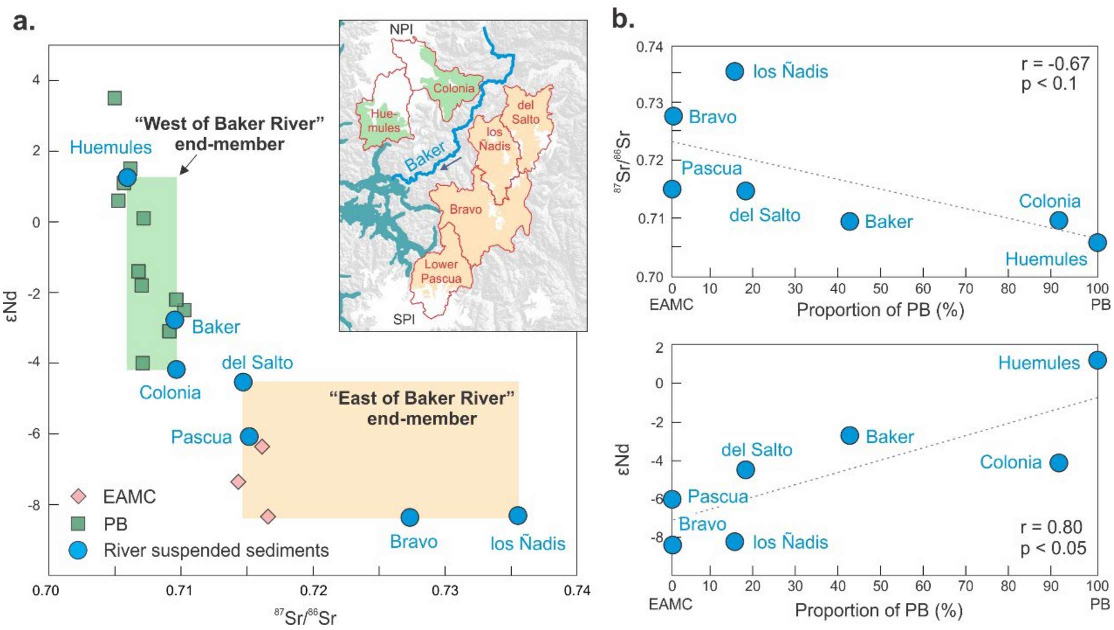

Figure 3. $^{87}Sr/^{86}Sr$ and εNd composition of the river suspended sediment samples and comparison with the isotopic signature of the dominant bedrock lithologies (cf. Table 1). **(a)** $^{87}Sr/^{86}Sr$ and εNd compositions of the river suspended sediments samples compared to those of the Patagonian Batholith (PB) (Pankhurst et al., 1999) and Eastern Andean Metamorphic Complex (EAMC) (Weaver et al., 1990). **(b)** Isotopic signatures ($^{87}Sr/^{86}Sr$ and εNd) of the river suspended sediments plotted against the relative areal proportion of the two main lithologies in their respective watersheds (Table 1). In all plots, the error bars are smaller than the size of the dots. In **(a)**, the $^{87}Sr/^{86}Sr$ and εNd signatures of the Huemules and Colonia river suspended sediment samples are used to characterize the "West of Baker River" end-member, which is dominated by the PB, whereas those from Pascua, del Salto, Bravo and los Ñadis rivers are used to define the "East of Baker River" end-member, which is dominated by the EAMC. The Baker River suspended sediment sample is not used to define sources since it represents a mixture of both sources. The source end-members are defined using the

isotopic range (min–max values; represented as colored rectangles) of the river suspended sediment samples. The sub-watersheds used to define the “West of Baker River” and “East of Baker River” end-members are represented on the inset map in green and peach, respectively.

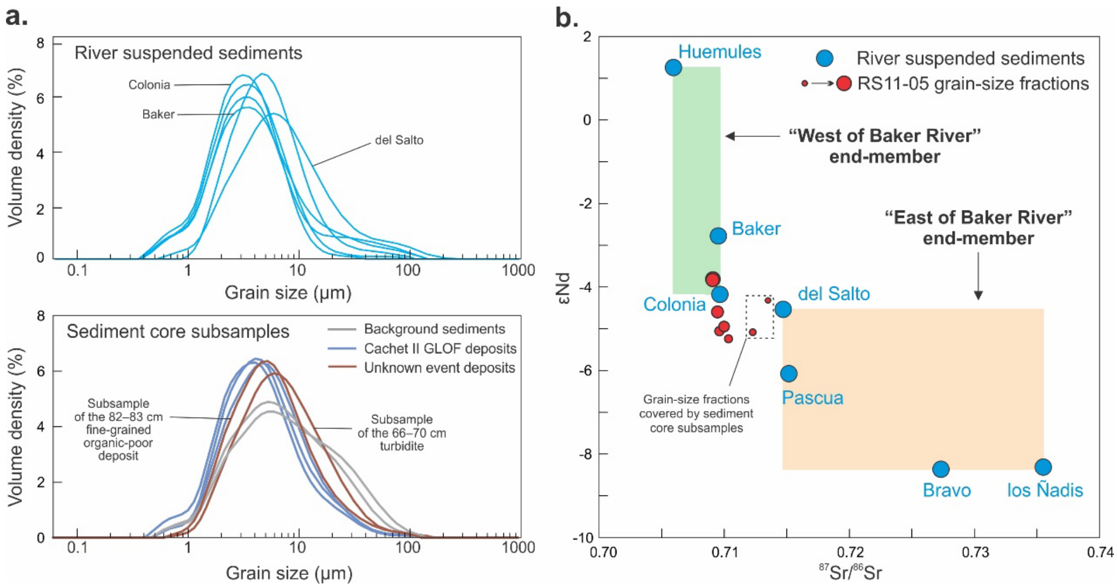

Figure 4. Evaluation of the influence of grain size on sediment provenance reconstruction. **(a)** Grain-size distributions of the river suspended sediments and of the FC17-08 sediment core subsamples. In **(b)**, the isotopic composition of the eight grain-size fractions (0–4, 4–8, 8–16, 16–32, 32–45, 45–63, 63–90, and 90–125 µm) of river sediment sample RS11-05 (red dots) are compared to the isotopic signature of the two source end-members (West vs. East of Baker River) defined in Figure 3. The error bars are smaller than the size of the dots. Note that most of the fjord sediment samples are finer than ~10 µm and therefore correspond in grain size to the two finest sub-samples from RS11-05.

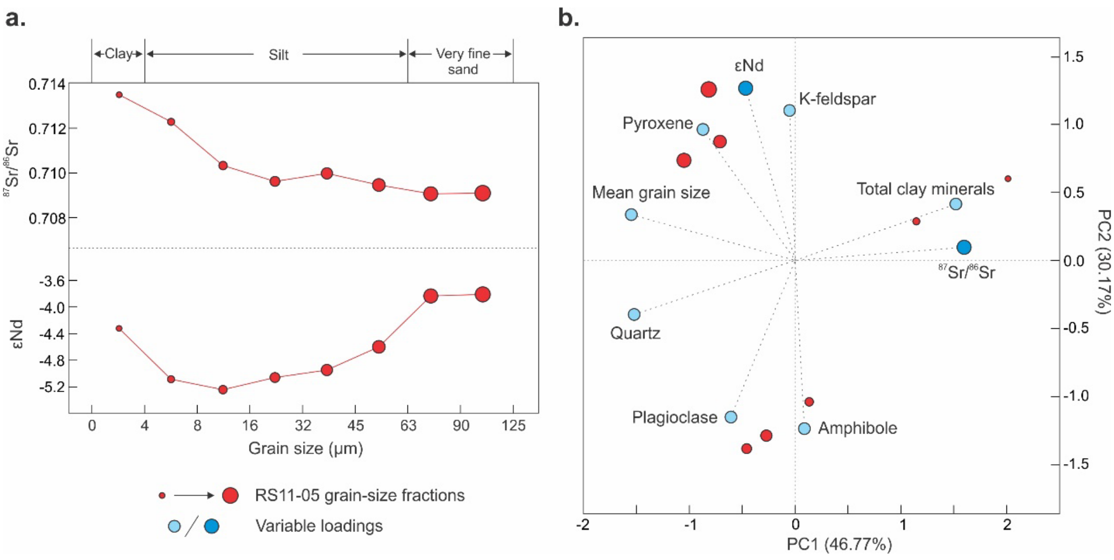

Figure 5. Variations in the $^{87}Sr/^{86}Sr$, εNd, and mineralogical composition of river sediment sample RS11-05 (Baker River) with grain size. **(a)** $^{87}Sr/^{86}Sr$ and εNd composition of the eight RS11-05 grain-size fractions plotted vs. grain size. The error bars are smaller than the size of the dots and are therefore not visible. **(b)** PCA biplot of $^{87}Sr/^{86}Sr$, εNd, grain-size mean, and mineralogy of the same eight grain-size fractions.

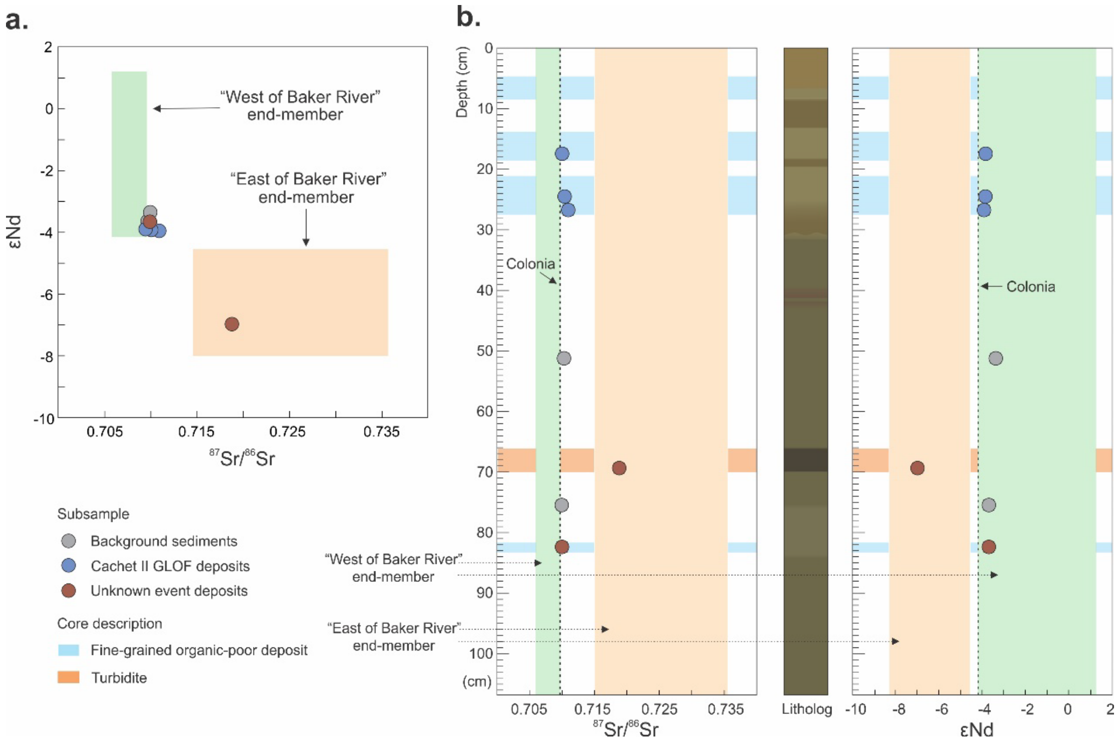

Figure 6. Provenance of the subsamples from sediment core FC17-08. The $^{87}Sr/^{86}Sr$ and εNd composition of the subsamples is **(a)** compared to the composition of the sources defined in Figure 3 (εNd vs. $^{87}Sr/^{86}Sr$ biplot), and **(b)** plotted against depth. The depth of the fine-grained organic-poor deposits identified by Vandekerkhove et al. (2021) is marked in blue and that of the turbidite is in orange. The isotopic values of the suspended sediment sample collected in proglacial river Colonia is indicated in **(b)** using dashed lines as this river is the outflow of proglacial lake Cachet II, which is at the origin of the 21st century Baker River GLOFs.

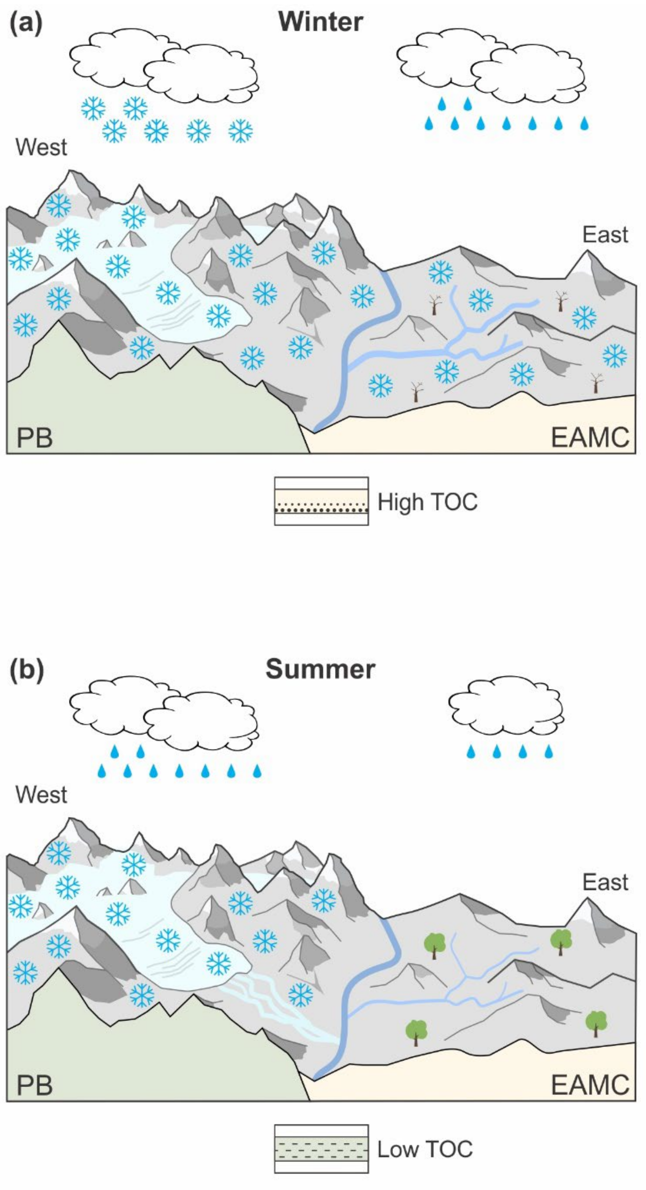

888 **Figure 7**. Schematic models illustrating the differences between rain-on-snow flood events
889 occurring in winter vs summer. **(a)** In winter, the entire watershed is snow-covered but
890 precipitation falls as snow in its western part. Therefore, rain-on-snow events primarily affect
891 the eastern part of the watershed and are recorded in downstream fjord sediments as intense
892 rainfall events, i.e., organic-rich turbidites of Eastern Andean Metamorphic Complex (EAMC)
893 origin. **(b)** In (early) summer, only the western part of the Baker River watershed is snow-

covered. Rain-on-snow events are therefore recorded in downstream fjord sediments as fine-grained organic-poor layers, representing glacial material of Patagonian Batholith (PB) origin.

Table 1. Proportions of the two main lithologies (Patagonian Batholith [PB] and Eastern Andean Metamorphic Complex [EAMC]) in the watersheds of the seven sampled rivers, based on SEGEMAR (1998), SERNAGEOMIN (2003), and Gómez et al. (2019). For the Baker and Pascua River watersheds, calculations were made for the lower parts the watersheds only since sediments derived from the upper sub-watersheds are filtered by lakes General Carrera and Cochrane, and by Lake O'Higgins, respectively (Figure 1). The lithology under the NPI was assumed to be entirely PB. Only the PB and EAMC lithologies were considered in the calculation since the other lithologies are limited to minor occurrences in the upper (drier) part of the lower Baker River sub-watershed along Chacabuco River (Fig. 1).

Watershed	Lithological proportion	
	PB (%)	EAMC (%)
Huemules	100	0
Colonia	91	9
Lower Baker	42	58
Del Salto	17	83
Los Ñadis	15	85
Bravo	1	99
Lower Pascua	0	100